ChemPhysChem | doi.org/10.1002/cphc.202000952

European Chemical Societies Publishing

Flow-driven Surface Instabilities of Tubular Chitosan Hydrogel

Pawan Kumar,[a] Cintia Hajdu,[a] Ágota Tóth,[a] and Dezső Horváth*[b]

Spatial structures break their symmetry under the influence of shear stress arising from fluid flow. Here, we present surface instabilities appearing on chitosan tubes when an acidic solution of chitosan with various molecular weight is injected into a pool of sodium hydroxide solution. At slow flow rates wrinkle-to-fold transition takes place along the direction of the flow yielding a banded structure. For greater injection rates we observe coexisting modes of wrinkles and folds which are stabilized to periodic wrinkles when the alkaline concentration is increased. The instabilities are characterized by the scaling laws of the pattern wavelength and amplitude with the tube characteristics. Our experimental adaptation of mechanical instabilities provides a new *in situ* method to create soft biomaterials with the desired surface morphology without the use of any prefabricated templates.

1. Introduction

Local interactions in non-equilibrium systems develop self-organized materials. Hence, structured hydrogels are very useful soft materials for drug delivery in biomedical sciences, flow actuators in microfluidics and even as sensors.[1,2] The chemical and physical properties of gels and their responsive nature with solvents[3–6] and stimuli like pH,[7] temperature,[8,9] light,[10–13] and electric potential[14] captivate the interest in organized pattern formations. The characteristic length associated with these patterns can range from micro to nano scale.[15] The patterning on the surface or at the interface of membranes due to an external or internal strain typically appears in the form of buckling instabilities like wrinkles and folds.[16–18] These structures are frequently found in natural systems as phyllotactic patterns on plants,[19] buckles and ridges on exocarps of fruits or vegetables,[20] and wrinkles on the skin.[21] Recently the periodic folding of brain organoids on a specially designed chip has also been observed.[22] To understand the underlying mechanism, extensive studies have been carried out from small to large scales. Control of length scales yields various promising applications in tunable optical and nano-devices,[23,24] flexible microelectronics,[25] ordering of liquid crystals,[26] microfluidic channels,[27] etc.

The transformation of mechanical surface instabilities has gained tremendous interest in the last few years.[16,28,29] Wrinkling can transform into folds under uni- or biaxial compressive strain on a membrane[30–34] or on granular rafts.[35] It has also been demonstrated that wrinkles form as first-order linear response and localize into folds by nonlinear effects of the membrane.[16,30] However, the evolution of patterns on an *in situ* forming interface via gelation has not been explored. The sol-gel-driven system provides flexibility in governing a variety of useful functional materials and can be beneficial in the development of adaptive materials.

Previously we have designed a method, utilizing laminar flow, to create chitosan gels in various structures resembling soft chemical gardens.[36] We have also determined the experimental conditions where the developing gel interface between acidic and alkaline solutions can go through spontaneous symmetry breaking of the smooth surface and chitosan tubes exhibiting well-defined periodic wrinkles arise. In this work, we apply the same flow-driven approach to explore the types of surface instabilities inherent in the system for chitosan tubes of various molecular weights. The evolving morphologies are controlled by the alkaline concentration and the flow rate of the chitosan solution.

Experimental Section

Analytical grade reagents, medium (Sigma-Aldrich 448877) and high molecular weight (Sigma-Aldrich 419419) of chitosan (CS), CH_3COOH (VWR, 99–100%), and NaOH (Sigma-Aldrich, pellets), were used for all the experiments. All solutions were prepared with deionized water (Purite RO100). For chitosan acidic solution, 0.75 g of medium molecular weight (MMW) and high molecular weight (HMW) of CS was added in 100 ml CH_3COOH (0.2 M) solution under stirring for 18 and 24 hours, respectively.

To perform the flow-driven experiments, a Plexiglas cuvette ($1\times 1.5\times 20$ cm^3) with inlet pinhole near the wall, was filled with 15 mL solution of NaOH with varying composition (0.75 M, 1.0 M, and 1.5 M). CS solution was then injected from below with a peristaltic

[a] P. Kumar, C. Hajdu, Á. Tóth
Department of Physical Chemistry and Materials Science, University of Szeged, Rerrich Béla tér 1, Szeged, H-6720, Hungary
[b] D. Horváth
Department of Applied and Environmental Chemistry, University of Szeged, Rerrich Béla tér 1, Szeged, H-6720, Hungary
E-mail: horvathd@chem.u-szeged.hu

Supporting information for this article is available on the WWW under https://doi.org/10.1002/cphc.202000952

pump (Ismatec Reglo) through a Tygon tube (i.d.: 1.42 mm) and inlet needle (i.d.: 0.60 mm) into the alkaline solution as shown in Figure 1. All experiments were performed at room temperature ($24 \pm 2\,^{\circ}C$).

An imaging system with a Unibrain fire-i 630c camera with Vivitar extension tubes was used to record the spatiotemporal pattern formation. The characteristics of the structures were determined by ImageJ software. The surface deformations led to spatial inhomogeneity with lighter and darker regions and the patterns were classified by visual inspection based on the geometry. The characteristic wavelength of these patterns (λ) was determined by averaging the interpeak distances of greyscale intensity profiles. The diameter d and the depth h of the tube (see Figure 1(b–c)) were calculated as the ratio of the area of the tube from the corresponding projection and the length of the tube. The thickening of the tube wall was monitored by the scattering of a green laser beam (Roithner LaserTechnik, $\lambda = 532$ nm, $P = 100$ mW) from the tube. The laser was mounted vertically such that the beam passed through a thin convex lens (Techspec), making 90° angle with the camera.

The viscosity of 500 mL of MMW and HMW chitosan solution was measured with a rotational viscometer (Anton Paar ViscoQC-300) and the density of the reactants with a density meter (Anton Paar DMA-500). The results are summarized in Table 1 along with the data for the NaOH solution.

2. Results and Discussion

When we inject an acidic chitosan solution from below into a pool of an alkaline solution, a polysaccharide membrane forms immediately around the injection point. An upward growing closed tube develops which adheres to the glass wall in accordance with our previous work.[36] At slow injection rates and high NaOH concentration, tubes with a smooth surface evolves as shown with filled circles in the dynamical phase diagram in Figure 2.

When the alkaline concentration is decreased and the flow rate is increased, narrow dark stripes appear on the tube transverse with right angle to the flow (open circles in Figure 2). Close inspection of the tubes reveals that the flat outer surface deforms and the periodic folds correspond to the dark bands. Their formation occurs via wrinkle-to-fold transitions illustrated in Figure 3(a–d) (see VideoS1 in SI). A wrinkle forms near the closed tip of the tube (Figure 3(b)) when the head expands and its size reaches a maximum. As the tube grows, the wrinkle deepens with increasing amplitude until it makes a self-contact as in Figure 3(c)) and a fold localizes into the surface (Figure 3(c)). To quantitatively describe the process, we measure the change in the position (Δ) of the wrinkle transforming to fold from Figure 3(a) to Figure 3(d) along the flow which shows a monotonic increase as a function of time (see Figure 3(e)). Once the next deformation arises, the position of the fold will not change resulting in a constant dark band.

The deformation is initiated near the edge where the tube wall is in contact with the rigid supporting boundary of the container. In thin cylinders with a p_i internal pressure, the circumferential stress ($\sigma_\theta = p_i d/(2w)$) is greater than the axial stress ($\sigma_z = p_i d/(4w)$), where w is the wall thickness.[38] Due to the larger strain in the xy-plane, therefore, surface depressions propagate along the outer surface transverse to the direction of the tube growth. Wrinkles then form on the surface in the center region of the chitosan tube wall, which will later develop into folds. Since this wrinkle-to-fold transition is responsible for the appearance of the periodic bands, one expects that the wavelength of the wrinkles will determine the periodicity of folds as well. Indeed, the characteristic wavelength of the folds in Figure 3(f) is a linear function of the tube depth, h (see

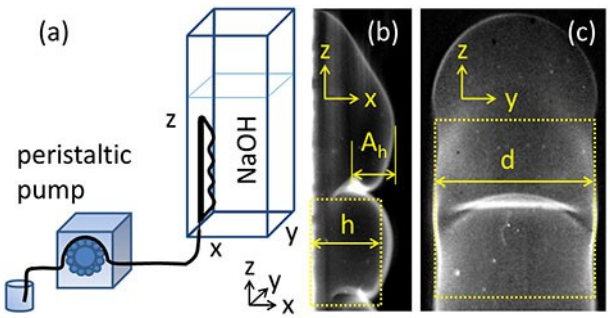

Figure 1. (a) Schematic diagram of the experimental setup. The side (b) and the front (c) view of a developing tube.

Table 1. The chemical composition of the chitosan MMW and HMW in 0.2 M CH_3COOH. Densities and viscosities of the reactants. The viscosities of the NaOH solution are from reference [37].

Name	Composition	ρ [g cm^{-3}]	η [mPa s]
MMW CS	0.75 w/V%	1.0013	71.71
HMW CS	0.75 w/V%	1.0012	138.8
NaOH	0.75 M	1.0283	0.9961
NaOH	1.0 M	1.0387	1.1042
NaOH	1.5 M	1.058	1.23

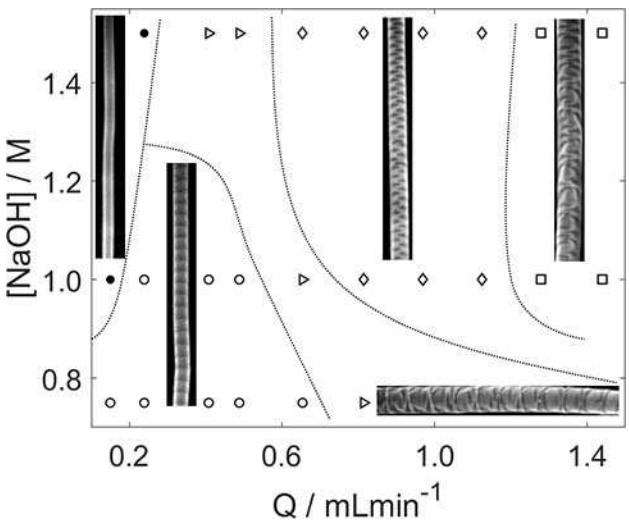

Figure 2. Dynamical phase diagram of the chitosan based hydrogel patterns for MMW chitosan. The field view of all images is 0.79×6.45 cm^2. The dotted curves are to guide the eye.

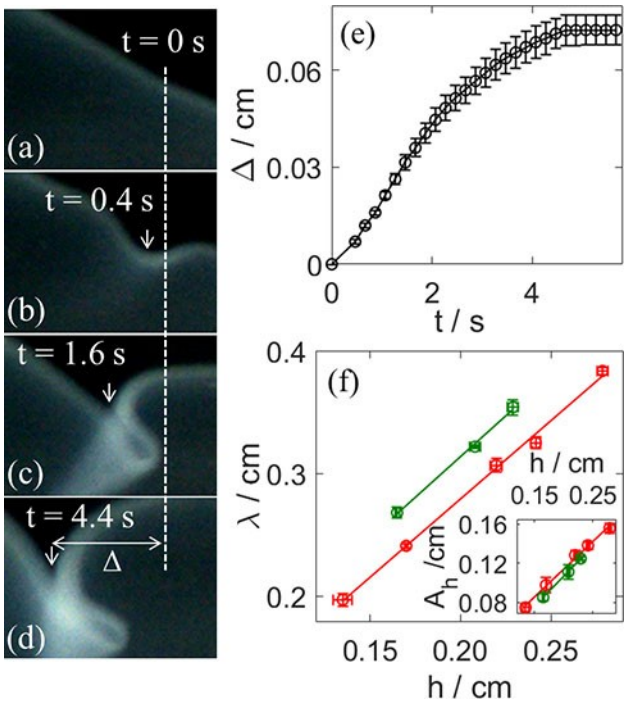

Figure 3. (a–d) Image sequence of wrinkle-to-fold transition of MMW with [NaOH] = 0.75 M, Q = 0.488 mL min^{-1}, and field view of 0.15 × 0.11 cm^2. (e) Temporal evolution of the change in position of the deformation. (f) Wavelength and amplitude (inset) of the folds as a function of tube depth *h* for [NaOH] = 0.75 M (red) and 1.0 M (green).

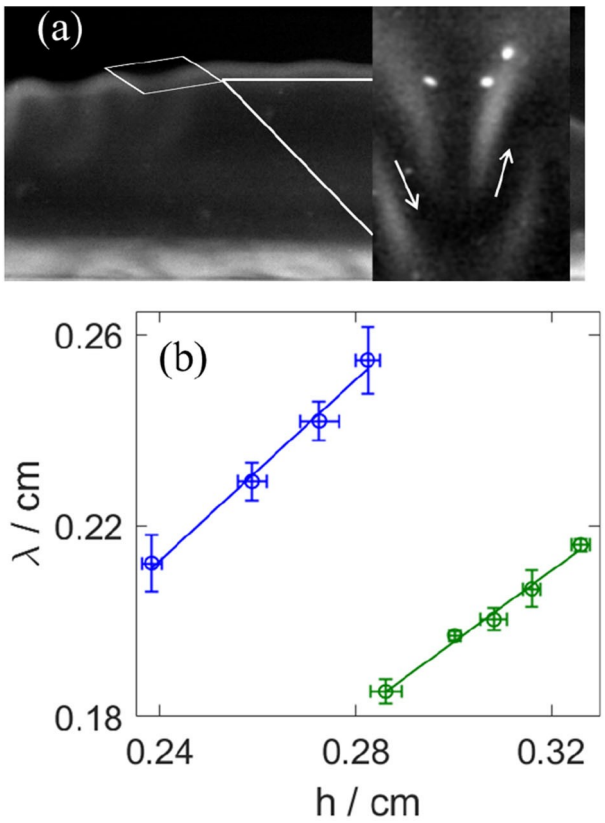

Figure 4. Front head of the wrinkling instability in the *x*–*z* plane (view: 0.77 × 0.36 cm^2) and enlarged section of the patterns in the *y*–*z* plane (field view: 0.23 × 0.35 cm^2) with Q = 0.97 mL min^{-1}. (b) Wavelength scales as a function of tube depth *h* at [NaOH] = 1.0 M (green) and 1.5 M (blue).

Figure 1(b) for definition) in good agreement with our previous work where we reported that the wavelength of wrinkling patterns on low molecular weight (LMW) tubes scales linearly with *h*.[36] The same dependence is observed for the fold amplitude (A_h), defined in Figure 1(b), in Figure 3(f).

Further increase of the flow rate increases the amplitude of local wrinkles which affects the tube deformation by allowing the coexistence of wrinkles and folds (see triangular markers in Figure 2). However, at higher NaOH concentrations, the mixed modes of the folding and wrinkling states are stabilized to regular wrinkling patterns. Stationary periodic wrinkling, characterized by a regular dark zigzag pattern and depicted by diamond markers in Figure 2, appears far from the tube tip. The deformations take place along the direction of the tube head with π phase shifting at the boundaries (Figure 4a, VideoS2 in SI), similarly to that observed using LMW chitosan.[36]

The characteristic wavelength in Figure 4(b) indicates the linear scaling as a function of tube depth, *h*, analogously to previous studies of wrinkling where wavelength is dependent on the thickness of the gel.[12] We have also found that the increase in the alkaline concentration increases the wavelength of surface deformations (cf. the blue and green symbols in Figure 4(b)). For wrinkling, the wavelength is shorter than that of folding. The further increase of the flow rate enhances the underlying strain on the edges, due to which irregularity emerges on the periodic wrinkling (square markers in Figure 2).

We have checked the changes in the phase diagram when chitosan solution with higher molecular weight is used. At higher alkaline concentration and low flow rate, straight tubes evolve with a uniform diameter (see filled circles in Figure 5), similarly to the MMW case summarized in Figure 2. At higher

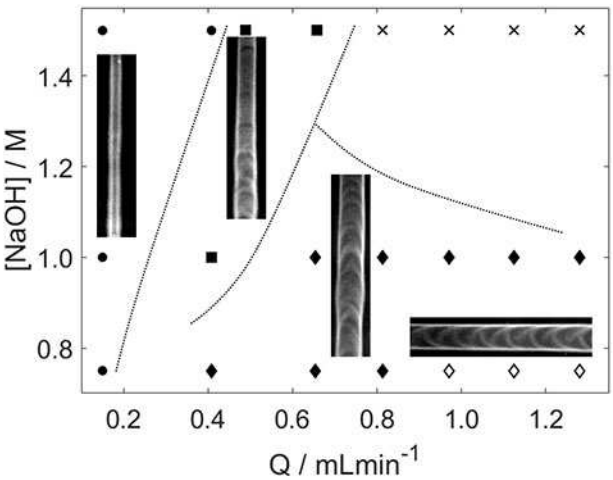

Figure 5. Dynamical phase diagram of the chitosan based hydrogel patterns for HMW chitosan. The field view of all images is 0.96 × 4.85 cm^2. The dotted curves are to guide the eye.

flow rates, the coexistence of flat tubes and wrinkling pattern is observed (see filled square markers in Figure 5). Further increase of the flow rates leads to wrinkling patterns as shown by diamond markers in Figure 5, while at higher NaOH concentration there is no tube formation (see cross marks).

We have determined the surface instabilities for CS hydrogels of different molecular weight and hence different physical properties. The viscosity of the CS solution increases on increasing the molecular weight of chitosan, while the density change is negligible (cf. Table 1). The increase in viscosity affects the tube growth and hence the surface instabilities. Comparing the two phase diagrams, the common features are clear. At constant chemical composition and hence constant density change, deformations appear on the smooth surface of the vertically growing tube giving rise to folding and wrinkling patterns when the injection rate of the acidic chitosan solution is increased. There is a distinct difference, however, as wrinkle-to-fold transition has not been observed for the HMW polymers. The main reason is that the HMW polymer solution is more viscous than the MMW, which affects the vertical motion of the tube. Its growth along the flow is quantitatively described by the linear velocity (v), which increases with the flow rate in Figure 6(a). The linear velocity is smaller for the HMW polymer because of their greater viscosity. The tube diameter (d) and the tube depth (h) are major characteristics of the tubes. They show a monotonic increase as a function of the injection rate in Figure 6(b–c) independent of the polymer molecular weight. The tube depth (h), however, is significantly lower for the MMW gels because of its higher linear velocity. The tube diameter $d \approx 2h$ that corresponds to a semi-cylindrical tube for MMW, while for HMW $d < 2h$ gives a highly distorted tube because of its stronger cohesion in the polymer network.[39] Figure 6 also indicates that these characteristics increase with decreasing the sodium hydroxide concentration, whereas the linear flow velocity decreases. At lower [NaOH], bouyancy is less, i.e., the density difference of the two reactants is smaller, resulting in a thicker tube. The volume growth rate (R) of the half cylindrical tubular structure is calculated using $R = \pi dhv/4$ and is found to be directly proportional to the flow rate, as presented in Figure 6(d). Despite the different tube characteristics, the slope of the $R - Q$ straight line is near unity for all the concentrations and molecular weights (for MMW: 1.03 ± 0.03 and for HMW: 0.98 ± 0.07). Thus, likewise the LMW scenario,[36] there is no significant liquid transfer through the hydrogel membrane.

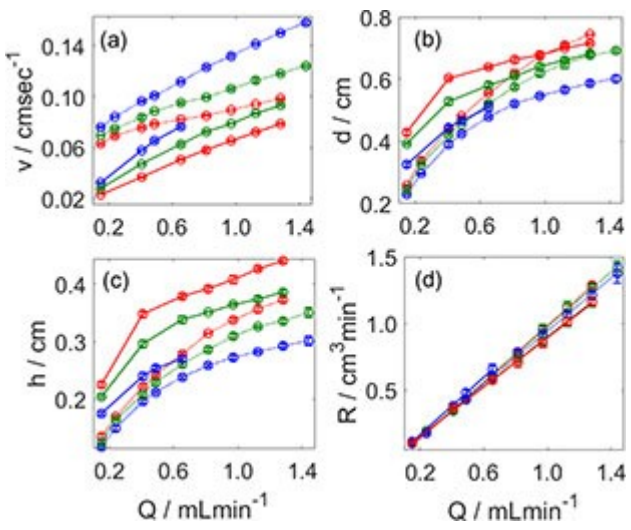

Figure 6. Characteristic properties of the tube as a function of flow rate: (a) linear velocity, (b) diameter, (c) depth, and (d) volume rate. For MMW (dotted) and HMW (solid), [NaOH] = 0.75 M (red), 1.0 M (green) and 1.5 M (blue).

Previously we have shown that the wall thickness (w) of the LMW chitosan tubes scales as $w = (kt)^{\alpha}$ for flow-driven gelation with an exponent of $\alpha = 0.5$ suggesting a diffusion-limited widening of the gel membrane.[36] Figure 7 illustrates that scaling can be applied for different chitosan hydrogels as well. The scaling exponents, summarized in Table 2, are determined as slopes of the logarithmic plots (see e.g. Figure 7b). It is found that on average $\alpha = 0.49 \pm 0.04$, which indicates that diffusion is the dominating transport process for increasing the wall thickness of the tube independent of the molecular weight. The decrease in the proportionality constant k is probably due to the faster gelation, and hence, slower transport through the membrane. The wall thickening also leads to decrease in the circumferential and axial stress in accordance with the evolution of the stationary patterns.

Finally, in comparison with LMW chitosan hydrogels,[36] periodic wrinkles are also established for MMW and HMW tubes but in different phase space regimes. New types of instabilities are observed for MMW and HMW as coexisting modes of wrinkles and folds are found to be only with MMW, while those

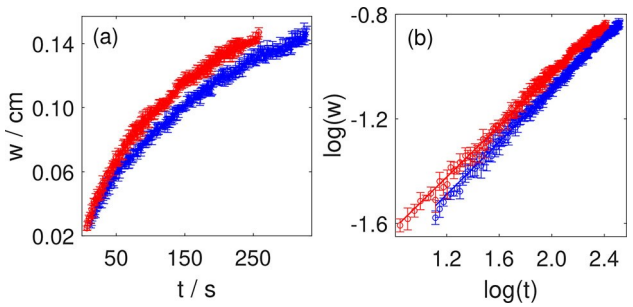

Figure 7. (a) Temporal evolution of the tube wall thickness and (b) log-log fitting for MMW (red) and HMW (blue). Conditions: [NaOH] = 1.0 M, Q = 0.970 mL min^{-1} (MMW) and Q = 0.408 mL min^{-1} (HMW).

Table 2. Temporal scaling exponents (α) and proportionality constants (k) for MMW with Q = 0.970 mL min^{-1} and HMW gels with Q = 0.408 mL min^{-1}.

Name	[NaOH] [M]	α	$10^5\ k$ cm$^{1/\alpha}$/s
MMW	0.75	0.53 ± 0.02	9.9 ± 0.5
HMW	0.75	0.53 ± 0.01	7.3 ± 0.2
MMW	1.0	0.49 ± 0.01	7.7 ± 0.1
HMW	1.0	0.50 ± 0.01	6.6 ± 0.2
MMW	1.5	0.45 ± 0.01	4.9 ± 0.1
HMW	1.5	0.44 ± 0.01	4.4 ± 0.3

of simple tubes and wrinkles are reported for HMW where greater viscosity suppresses the formation of finer patterns.

3. Conclusions

Boundary aided growth of tubular structures is exhibited for various chitosan polymers. Spontaneous symmetry breaking results in wrinkle-to-fold transition near the tip and wrinkles far from the tip. The wavelength of folds and wrinkles shows linear scaling with the tube depth. The concentration gradient between the injected and the outer liquid drives the sol-gel transition with temporal scaling revealing diffusion as the main mode of transport across the interface. Despite different characteristic properties of the tubular structures due to difference in viscosity and cohesive forces, the volume growth rate and the temporal scaling of the thickening of tube wall are observed to be similar for the polymers independent of their molecular weight. Our experimental findings of the self-organized surface deformations of chitosan hydrogels not only add a new insight into the localization of buckling instability, but also open new possibilities for the design of adaptive soft materials under biomimetic conditions *via* the simple control over patterning. Furthermore, the separation of the reacting electrolytes to different compartments endows the feasibility to measure the electric potential of the *in situ* prepared organic membranes.

Acknowledgement

This work was supported by the National Research, Development and Innovation Office (NN125746), GINOP-2.3.2-15-2016-00013, University of Szeged Open Access Fund (5140) and M-ERA.net MaSNEC projects.

Conflict of Interest

The authors declare no conflict of interest.

Keywords: chitosan · hydrogel · membrane · self-organization · surface instabilities

[1] N. Bhattarai, J. Gunn, M. Zhang, *Adv. Drug Delivery Rev.* **2010**, *62*, 83–99.
[2] H. Banerjee, M. Suhail, H. Ren, *Biomimetics* **2018**, *3*, 15.
[3] T. Tanaka, S. T. Sun, Y. Hirokawa, S. Katayama, J. Kucera, Y. Hirose, T. Amiya, *Nature* **1987**, *325*, 796–798.
[4] E. S. Matsuo, T. Tanaka, *Nature* **1992**, *358*, 482–485.
[5] H. Lee, J. Zhang, H. Jiang, N. X. Fang, *Phys. Rev. Lett.* **2012**, *108*, 214304.
[6] S. Hirotsu, *J. Chem. Phys.* **1988**, *88*, 427–431.
[7] M. Leocmach, M. Nespoulous, S. Manneville, T. Gibaud, *Sci. Adv.* **2015**, *1*, e1500608.
[8] J. Kim, J. Yoon, R. C. Hayward, *Nat. Mater.* **2010**, *9*, 159–164.
[9] Z. Hu, Y. Chen, C. Wang, Y. Zheng, Y. Li, *Nature* **1998**, *393*, 149–152.
[10] J. Yoon, P. Bian, J. Kim, T. J. McCarthy, R. C. Hayward, *Angew. Chem. Int. Ed.* **2012**, *51*, 7146–7149; *Angew. Chem.* **2012**, *124*, 7258–7261.
[11] A. W. Hauser, A. A. Evans, J. H. Na, R. C. Hayward, *Angew. Chem. Int. Ed.* **2015**, *54*, 5434–5437; *Angew. Chem.* **2015**, *127*, 5524–5527.
[12] E. P. Chan, E. J. Smith, R. C. Hayward, A. J. Crosby, *Adv. Mater.* **2008**, *20*, 711–716.
[13] J. Dervaux, M. B. Amar, *Annu. Rev. Condens. Matter Phys.* **2012**, *3*, 311–332.
[14] E. Schäeffer, T. Thurn-Albrecht, T. P. Russell, U. Steiner, *Nature* **2000**, *403*, 874–877.
[15] B. A. Grzybowski, *Chemistry in Motion: Reaction-Diffusion Systems for Micro- and Nanotechnology*, Wiley, Chichester, **2008**.
[16] L. Pocivavsek, R. Dellsy, A. Kern, S. Johnson, B. Lin, K. Y. C. Lee, E. Cerda, *Science* **2008**, *320*, 912–916.
[17] P. Kim, M. Abkarian, H. A. Stone, *Nat. Mater.* **2011**, *10*, 952–957.
[18] B. Li, F. Jia, Y.-P. Cao, X.-Q. Feng, H. Gao, *Phys. Rev. Lett.* **2011**, *106*, 234301.
[19] P. D. Shipman, A. C. Newell, *Phys. Rev. Lett.* **2004**, *92*, 168102.
[20] J. Yin, Z. Cao, C. Li, I. Sheinman, X. Chen, *Proc. Nat. Acad. Sci.* **2008**, *105*, 19132–19135.
[21] K. Efimenko, M. Rackaitis, E. Manias, A. Vaziri, L. Mahadevan, J. Genzer, *Nat. Mater.* **2005**, *4*, 293–297.
[22] E. Karzbrun, A. Kshirsagar, S. R. Cohen, J. H. Hanna, O. Reiner, *Nat. Phys.* **2018**, *14*, 515–522.
[23] W. H. Koo, S. M. Jeong, F. Araoka, K. Ishikawa, S. Nishimura, T. Toyooka, H. Takezoe, *Nat. Photonics* **2010**, *4*, 222.
[24] L. Zhang, X. Lang, A. Hirata, M. Chen, *ACS Nano* **2011**, *5*, 4407–4413.
[25] J. Tang, H. Guo, M. Zhao, J. Yang, D. Tsoukalas, B. Zhang, J. Liu, C. Xue, W. Zhang, *Sci. Rep.* **2015**, *5*, 16527.
[26] R. Verduzco, G. Meng, J. A. Kornfield, R. B. Meyer, *Phys. Rev. Lett.* **2006**, *96*, 147802.
[27] D. J. Beebe, J. S. Moore, J. M. Bauer, Q. Yu, R. H. Liu, C. Devadoss, B.-H. Jo, *Nature* **2000**, *404*, 588–590.
[28] D. P. Holmes, A. J. Crosby, *Phys. Rev. Lett.* **2010**, *105*, 038303.
[29] A. T. Oratis, J. W. M. Bush, H. A. Stone, J. C. Bird, *Science* **2020**, *369*, 685–688.
[30] F. Brau, P. Damman, H. Diamant, T. A. Witten, *Soft Matter* **2013**, *9*, 8177–8186.
[31] P. Ciarletta, *J. Mech. Phys. Solids* **2014**, *73*, 118–133.
[32] M. Rivetti, *C. R. Mec.* **2013**, *341*, 333–338.
[33] S. Yu, Y. Sun, S. Li, Y. Ni, *Soft Matter* **2018**, *14*, 6745–6755.
[34] Y.-P. Cao, B. Li, X.-Q. Feng, *Soft Matter* **2012**, *8*, 556–562.
[35] E. Jambon-Puillet, C. Josserand, S. Protiere, *Phys. Rev. Mater.* **2017**, *1*, 042601.
[36] P. Kumar, D. Horváth, Á. Tóth, *Soft Matter.* **2020**, *16*, 8325–8329.
[37] J. R. Bourne, P. Dell'Ava, O. Dossenbach, T. J. Post, *J. Chem. Eng. Data* **1985**, *30*, 160.
[38] M. Kiehl, V. Kaminker, J. Pantaleone, P. Nowak, A. Dyonizy, J. Maselko, *Chaos* **2015**, *25*, 064310.
[39] C. Lim, D. W. Lee, J. N. Israelachvili, Y. Jho, D. S. Hwang, *Carbohydr. Polym.* **2015**, *117*, 887–894.

Manuscript received: November 18, 2020
Revised manuscript received: December 21, 2020
Accepted manuscript online: December 23, 2020
Version of record online: January 27, 2021